Memoirs of the Faculty of Engineering, Kyushu University, Vol.69, No.3, September 2009

Yielding Mechanism of Highly Perfect Copper Single Crystals

by

Sadakichi KITAJIMA*, Hiroaki KURISHITA** and Yuichi SAKURAI***

(Received August 3, 2009)

Abstract

In order to understand the yielding mechanism of highly perfect copper crystals, the behavior of dislocation multiplication has been investigated using etch pit techniques for crystals with few sub-grain boundaries and low initial dislocation densities from 3.4×10^2 to 8.3×10^3 cm^{-2}. Main results and conclusions are: The initiation of dislocation multiplication and the controlling mechanism of τ_m are strongly dependent on the ease of the pre-yield motion of grown-in dislocations. In crystals where grown-in surface dislocations are weakly pinned, a secondarily formed screw dislocation that terminates at the free side surface and contains no super-jogs acts as a trigger source responsible for the initiation of dislocation multiplication. In this case, the value of τ_m is controlled by a thermally activated process of the non-conservative motion of jogs of the leading screw dislocation multiplied from the trigger source. In crystals where grown-in edge dislocations are strongly pinned, yielding begins after unpinning of grown-in surface 30°screw dislocations and τ_m is determined by the length of free segments between super-jogs of grown-in screw dislocations. The propagation of dislocation multiplication onto the neighboring parallel slip planes is triggered by dislocation sources produced through the double cross-slip of screw dislocations on the free surfaces.

Keywords: Copper, Plastic deformation, Yield stress, Deformation mechanism, Etch pit, Dislocation, Multiplication

1. Introduction

In order to elucidate the mechanism of plastic yielding of fcc copper single crystals, many studies on the dislocation behavior in the very early stage of deformation have been performed by using dislocation etch pit techniques and X-ray topography methods [1~24]. One of the authors (SK) and his group have studied the macroscopic yielding of highly perfect copper crystals having no or few sub-boundaries by using dislocation etch pit techniques**.** According to their results, the macroscopic yielding of highly copper crystals without sub-grain boundaries proceeds from planer dislocations multiplication on single slip planes followed by their propagation onto the neighboring parallel slip planes [5,10,13,14,16,18]. The macroscopic critical resolved shear stress (yield strength) of the crystals is corresponding to the shear stress required for dislocation multiplication to initiate, τ_m, [16] under which an array or a few arrays of etch pits corresponding to multiplied dislocations are at first observed on a {111} surface. Furthermore, sub-grain boundaries impede the movement of grown-in and multiplied dislocations and interfere with the elucidation.

Based on those results, KS and his group have further insisted the importance of making clear the following items: those are, (1) the role on the pre-yield motion of grown-in dislocations on the initiation of

---

* Professor Emeritus, Kyushu University

**Associate Professor, International Research Center for Nuclear Materials Science, Institute for Materials Research (IMR), Tohoku University

***Office Manager of Genkai Nuclear Power General Office, Nishinippon Plant Engineering and Construction Co., Ltd.

dislocation multiplication, including the character of dislocation sources responsible for the initiation of dislocation multiplication, and (2) the controlling mechanism of the multiplication stress, τ_m, that is equal to the yield stress and (3) the character of dislocation sources for the propagation of dislocation multiplication onto the neighboring parallel slip planes.

Stimulated by their suggestion, the present authors have examined the pre-yield motion of individual grown-in dislocations with edge and 30°screw orientations emerging on the free {111} surfaces up to τ_m [21,22] and the behavior of planer dislocations multiplication and their propagation around τ_m by refined etch pit techniques [19] in order to clarify the items (1)-(3). They have made a preliminary report that describes each of the items [23]. Although the report includes some essential results for understanding of the items, it does not provide information required for comprehensive understanding of the items and thus the yielding mechanism of highly perfect copper crystals.

This paper presents the yielding mechanism of highly perfect copper crystals through the above items of all descriptions which are based on a thorough examination of many experimental results obtained so far on the pre-yield motion of all of the grown-in surface edge and 30°screw dislocations, planer dislocations multiplication and their propagation by using refined etch pit techniques. .

2. Experimental

Copper single crystal rods were grown by the Bridgemann technique with copper plates (99.998% purity) put in a graphite mold (ashes less than 20ppm) under a vacuum of $1x10^{-3}$Pa. These rods were shaped into tensile specimens with two different geometries as shown in **Fig. 1** by using strain-free acid cutting and polishing techniques. The tensile specimens had a rectangular or parallelsoidal cross-section with a longitudinal axis parallel to <123> or <110>, which were designated to as 123-Specimen or 110P-Specimen, respectively. The 123-Specimen and 110P-Specimen had respectively two or four {111} surfaces so that dislocations emerge as etch pits.

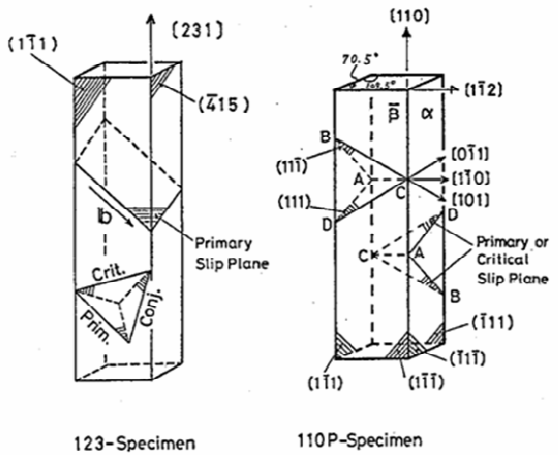

Fig. 1 Geometrical relationships among tensile axis, slip planes, slip directions and surfaces in specimens used.

The tensile specimens were subjected to thermally cyclic annealing [20] in a 2-hour cycle between 1150 and 1348K for 2 weeks, which enabled to prepare highly perfect copper crystals with no or few sub-boundaries and very low dislocation densities. Two different annealing atmospheres were used: a purified He atmosphere with an oxygen partial pressure less than 10^{-8} Pa and vacuum (1 mPa) with a higher oxygen partial pressure. Dislocations emerging on the {111} surfaces were observed as etch pits providing that the surfaces were exactly parallel to the {111} planes and etched with suitable dislocation etchants. **Table 1** lists the specimen, orientation of the specimen axis, dimensions, initial dislocation density, distribution of sub-boundaries and annealing atmosphere. For some specimens the surface was removal by electro-polishing after annealing, and the amount of surface removal which was previously confirmed to significantly affect the pre-yield motion of grown-in surface dislocations [21] is also shown in **Table 1**.

Table 1 Descriptions of the specimens used.

Specimen	Orientation	Dimension (mm^3)	N_0 (cm^{-2})	Sub-boundaries	Annealing atmosphere	Surface removal
U·123-1	<123>	3.2 x 3.1 x 30	8.3×10^3		Vacuum	100 μm
U·123-2	<123>	3.5 x 3.4 x 30	7.3×10^2		Purified He	0 μm
U·123-4	<123>	3.5 x 3.5 x 29	2.0×10^3		Purified He	0 μm
U·123-6	<123>	2.7 x 3.5 x 27	8.3×10^2		Purified He	0 μm
U·123-8	<123>	2.7 x 3.4 x 25	2.0×10^3		Purified He	0 μm
U·123-9	<123>	3.2 x 3.1 x 35	2.3×10^3		Vacuum	0 μm
U·123-10	<123>	3.6 x 3.7 x 44	5.6×10^2		Purified He	100 μm
U·110-1	<110>	2.8 x 2.6 x 34	2.8×10^3		Vacuum	100 μm
U·110-2	<1-10>	3.1 x 2.8 x 32	3.4×10^2		Purified He	0 μm

In order to apply tensile stresses to the specimens at room temperature and 77K, we used the dead-load application methods that allowed a precise control of applied stresses as small as 1 kPa. Before and after each of small load applications, the specimens were immersed into dislocation etchants and followed by taking optical micrographs over the entire areas of the two or four {111} surfaces. The positions of all of the grown-in edge and 30° screw dislocations emerging on the two or four {111} surfaces were recorded as dislocation etch pits with use of [A][19] and Livingston dislocation etchants[25] which differentiated the character (edge or 30°screw) and sign (plus or minus edge) of dislocations, respectively. These successive records of dislocation positions after every stress application required multiple etching techniques without any surface removal by electro-polishing throughout the experiments.

3. Results

3.1 Initiation of dislocation multiplication

In order to make clear the character of trigger dislocation sources responsible for the initiation of dislocation multiplication, and the controlling mechanism of the multiplication stress, τ_m, nine specimens with the initial dislocation densities, ρ_0, from 3.4×10^2 to $8.3 \times 10^3 cm^{-2}$ were subjected to the dead-load application at room temperature and 77K. In this section we present the effects of initial dislocation density, ρ_0, and temperature on the value of τ_m which are essential to understand the controlling mechanism of τ_m. The character of trigger dislocation sources will be discussed later.

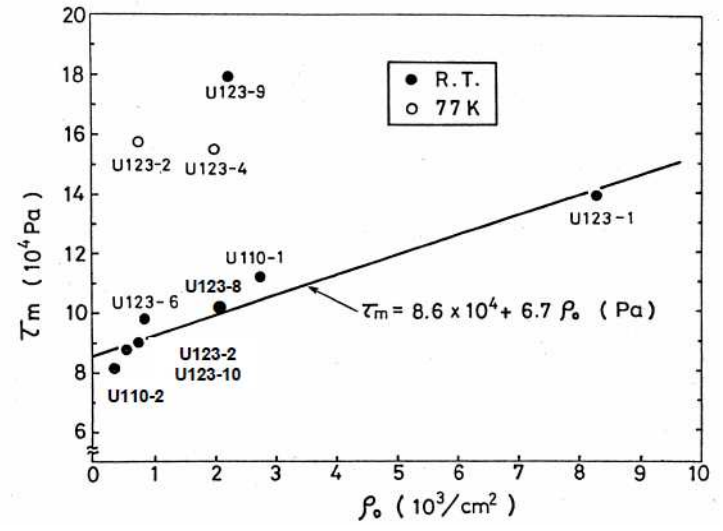

Fig. 2 Relationship between the multiplication stress, τ_m, and the initial dislocation density, ρ_0, for the specimens tested at room temperature and 77K.

The value of τ_m was determined as the applied shear stress at which an array or a few arrays of etch pits corresponding to multiplied dislocations appeared on a {111} surface. **Figure 2** shows the plot of τ_m against ρ_0 for the nine specimens measured at room temperature and 77K. At room temperature, the value of τ_m increases with increasing ρ_0, although there is one exception of U123-9. If we assume a linear relation between τ_m and ρ_0 at room temperature for the specimens except for U123-9, the following relationship is obtained,

$$\tau_m = 8.6x10^4 + 6.7\rho_0 \quad \text{(Pa)}. \tag{1}$$

On the other hand, the value of τ_m of U123-9 is significantly deviated upwards from eq. (1) and reaches approximately $16x10^4$ Pa, which is *1.8 times* as large as the values expected from eq. (1). In order to make clear the reason for the quite different behavior between U123-9 and the rest, a thorough comparison about the dislocation motion in every specimen was made at stresses up to τ_m. The followings are main characteristics of the results:

(1) All of the specimens satisfying eq. (1) exhibit glide motion of the grown-in surface edge and 30˚screw dislocations at very low stresses of below τ_m ($\tau = 0.1\,\tau_m$~$1.0\,\tau_m$), with much longer distances by the edge dislocations than those by the 30˚screw ones. The grown-in dislocations emerging on the surfaces of the specimens are most probable to be unpinned or very weakly pinned by impurities such as Cu_2O prior to load application. Because those specimens were subjected to either thermally cyclic annealing in the purified helium atmosphere or surface removal by electro-polishing after vacuum annealing at $1x10^{-3}$Pa.

(2) In U123-9 of which τ_m exhibits a large deviation from eq. (1), the grown-in 30˚screw dislocations first move at a stress of $\tau = \sim(2/3)\tau_m$; however, no grown-in edge dislocations moved even at $\tau = \sim \tau_m$. The grown-in dislocations, especially having the edge character are reasonably concluded to be strongly pinned prior to tensile loading; this specimen was subjected to thermally cyclic annealing in vacuum and followed by dead-loading without surface removal after annealing.

From the results mentioned above, it is reasonable to state that τ_m is strongly affected by the ease of movement of grown-in surface dislocations: In the case of the specimens where grown-in surface edge dislocations can move long distances at low stresses below τ_m, the values of τ_m are low and related to ρ_0 by eq. (1).

The data points obtained at 77K for U123-2 and U123-4 are shown in **Fig. 2**, where τ_m at room temperature also follows eq. (1). As is obvious from **Fig. 2**, the values of τ_m at 77K are significantly higher than those at room temperature. In these specimens long-distance movements of grown-in surface edge dislocations below τ_m were observed at 77K. These results indicate that τ_m for the specimens where the grown-in surface edge dislocations move long distance at low stresses below τ_m, depends on test temperature and thus τ_m is controlled by a thermally activated process.

When τ_m is controlled by a thermally activated process, τ_m is expected to depend not only on the test temperature, but also on loading time during dead-loading. **Figure 3** shows variations in the appearance of dislocation multiplication with loading time for U123-2 at room temperature. **Figure 3(a)** shows etch-pit arrays appearing on the $(1\bar{1}1)$ surface when the stress was applied at $\tau = \sim\tau_m$ for 20 seconds. The arrays of small etch-pits, which correspond to those of multiplied dislocations, at first appeared along the intersection between the primary slip plane and $(1\bar{1}1)$ surface after stressing $\tau = 9.0x10^4$Pa for 20 seconds, indicating $9.0x10^4$Pa to be τ_m. The small etch-pits were formed by two-fold etching with [A] etchant and then Livingston etchant, whereas the large etch-pits were corresponding to grown-in dislocations in the specimen subjected to nine-fold etching.

Figure 3(b) shows the dislocation distribution in the same area as **Fig. 3(a)** under the stress of $9.0x10^4$Pa (= $\sim\tau_m$) for further 130 second (totally 150 seconds). A new array of multiplied dislocations appears in the areas where no dislocation arrays are seen in **Fig. 3(a)**. It should be noticed that the new dislocation array was formed independently of the pre-existing multiplied dislocations. The propagation of dislocation multiplication also occurred onto the neighboring parallel slip planes, resulting in bands of multiplied dislocations, so that both the initiation and propagation of dislocation multiplication were dependent on loading time.

Figure 3(c) shows the distribution of multiplied dislocations on the $(\bar{1}1\bar{1})$ surface which is the reverse of the $(1\bar{1}1)$ surface shown in **Fig. 3(b)**. Comparison of **Figs. 3(b)** and **3(c)** proves that each of the multiplied dislocation bands exhibits a good correspondence between the two surfaces. As seen from an

enlarged micrograph of the two opposite surfaces (**Fig. 3(d)**), the contrast of outer part of the etch-pits formed by [A] etchant is bright and that of inner part of the etch-pits by Livingston etchant is dark, indicating all the multiplied dislocations to be the edge orientation with the same sign. In view of the cause of the contrast due to Livingston etchant and the fact that the angle between the primary slip plane and the {111} surfaces is either obtuse or acute, we can say that the arrays of multiplied edge dislocations distributing as etch-pits from edge to edge on the $(1\bar{1}1)$ or $(\bar{1}1\bar{1})$ surface do not extend on the primary slip planes from the $(1\bar{1}1)$ surface to the reverse $(\bar{1}1\bar{1})$ surface. This is important evidence that the screw components of the multiplied dislocations move considerably slower than the edge components.

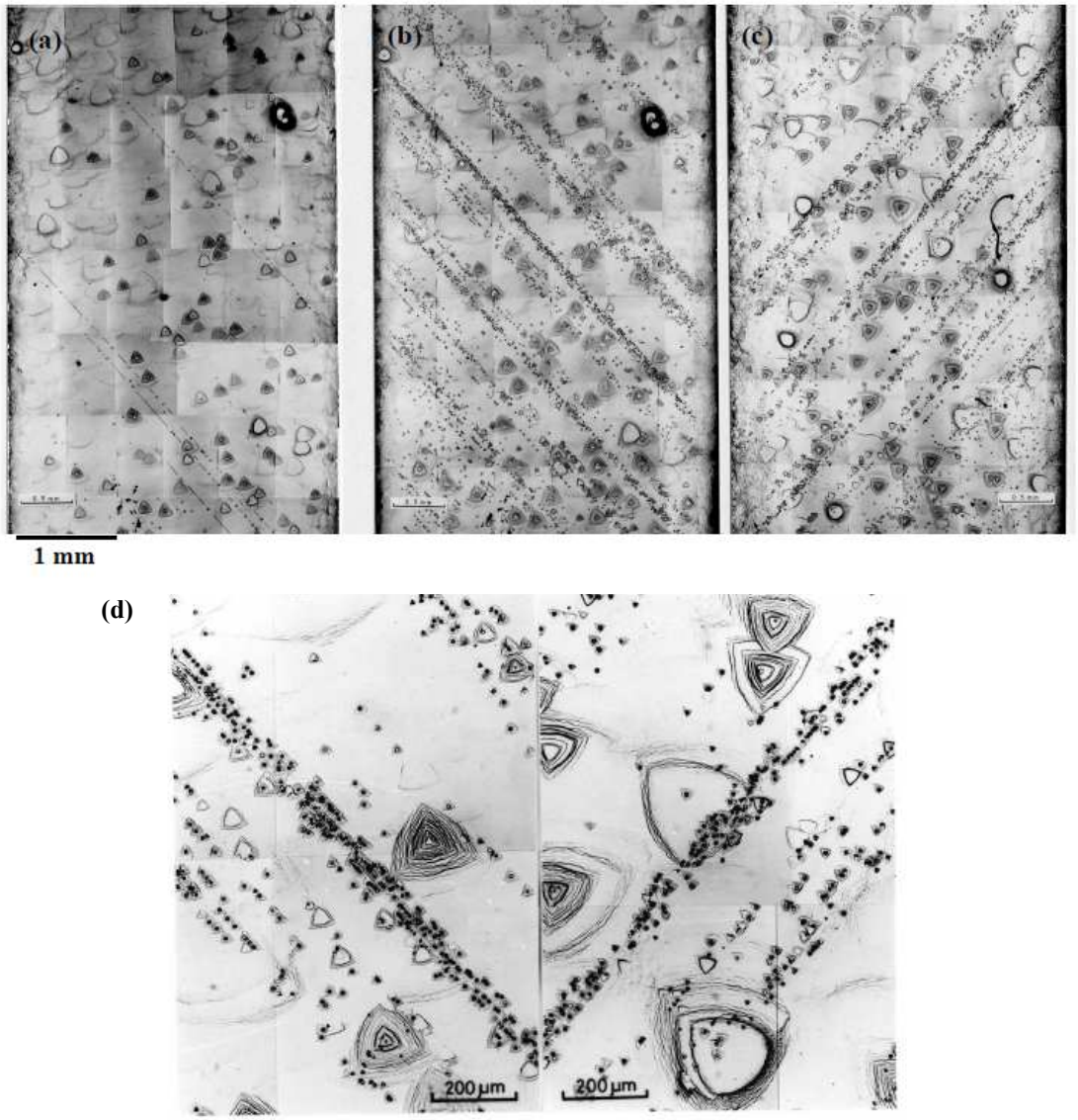

Fig. 3 Effects of loading time on the appearance of dislocation multiplication at room temperature for specimen U123-2. (a) shows several arrays of multiplied edge dislocations appearing on the $(1\bar{1}1)$ surface under a stress of $9.0\text{x}10^4$Pa ($\sim\tau_m$) for 20 seconds. (b) and (c) show arrays of multiplied edge dislocations appearing in the same area as (a) and on the reverse surface $(\bar{1}1\bar{1})$, respectively, under the stress of $9.0\text{x}10^4$Pa ($\sim\tau_m$) for 150 seconds. (d) is enlarged micrographs of the areas in (b) and (c).

3.2 Propagation of dislocation multiplication

Figure 4 shows the propagation of dislocation multiplications onto the neighboring parallel slip planes for U123-2 at room temperature. **Figure 4(a)** shows an array of multiplied dislocations (#1~#10) lying on the primary slip planes that appeared under the stress of 9.0×10^4Pa (= $\sim\tau_m$) for 20 seconds. The multiplied dislocations were subjected to 2-fold etching by [A] and Livingston etchants. The contrasts of both the outer and inner parts of all the etch-pits are bright, indicating that all the multiplied dislocations are the edge orientations with the same sign [19], where the extra-half plane exists at the side of the obtuse angle between the primary slip plane and $(1\bar{1}1)$ surface. From this result and the expected direction of specimen shearing under tensile loading, the moving direction of the multiplied edge dislocations is identified to be the direction marked by an arrow. In addition, individual edge dislocations in each array do not lie on a single slip plane, but lie on the neighboring parallel slip planes, indicating that the dislocation sources do not stay and continue to work on single slip planes, but change their slip planes by slightly shifting to the directions perpendicular to the original ones.

Figure 4(b) shows the dislocation distribution under the stress of 9.0×10^4 Pa ($\sim\tau_m$) for further 130 seconds. The area is corresponding to the same as in **Fig. 4(a)**. The edge dislocation array (#1~#10) moves on the primary slip plane and reaches the right side {145} surface where the primary screw dislocations emerge. Then, the primary edge dislocation arrays of the opposite sign (dark etch pits) are multiplied in band forms on the neighboring parallel slip planes. The traveling direction of the arrays is from the right side surface to the left, as indicated by an arrow in **Fig. 4(b)**. It is therefore concluded that when the edge components of dislocations multiplied from the trigger source reach the side {145} surface and emerge there as elongated screw dislocations, each of the screw dislocations acts as a new dislocation source and causes propagation of dislocation multiplication on the neighboring parallel slip planes.

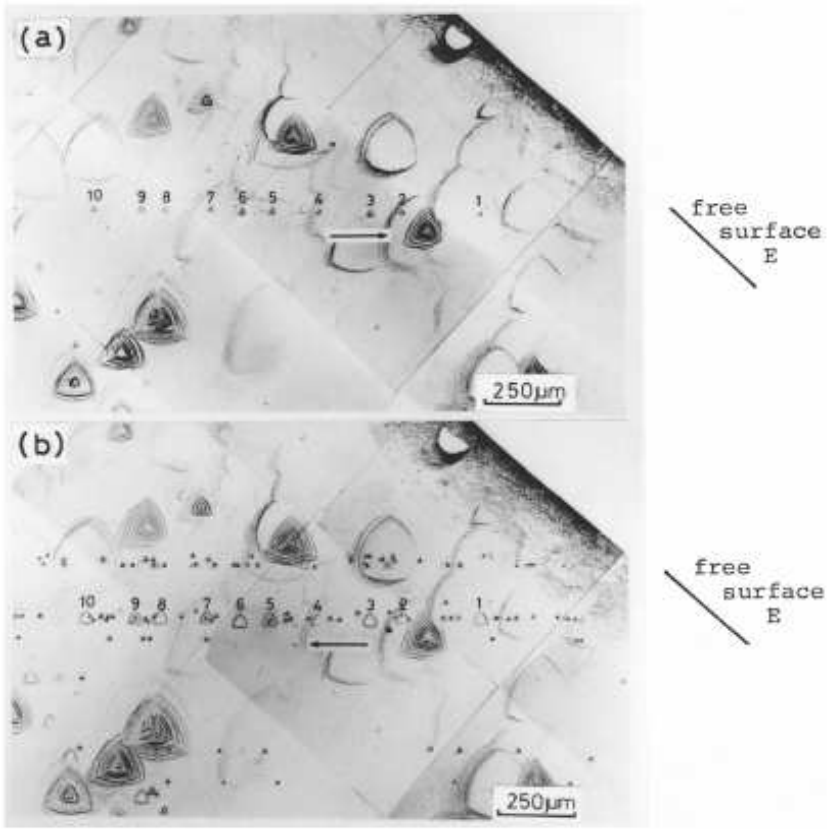

Fig. 4 Dislocation multiplication on close, several slip planes and the role of free surface E for specimen U123-2 under the stress of 9.0×10^4Pa (a) for 20 seconds and (b) for 150 seconds at room temperature.

Figure 5(a) shows the distribution of multiplied dislocations on the $(1\bar{1}1)$ surface of U123-6 that

appeared under a stress of 10.6×10^4Pa for 20 seconds after determining the value of τ_m (= 9.8×10^4Pa) at room temperature. The horizontal direction of the figure is parallel to the specimen longitudinal axis and the bottom of the figure is corresponding to the area near one of the $(1\bar{1}1)$ surface edges. Near the edge of the specimen, many streamers are seen and are composed of edge dislocations of opposite signs (bright and dark pits) interacting with each other and locating at approximately 45 degrees in a close distance, as seen in the figure. All of the bright-pit arrays in the streamers have the extra-half planes existing at the side of the obtuse angle between the primary slip plane and the $(1\bar{1}1)$ surface, whereas all of the dark-pit arrays in the streamers have the extra-half planes existing at the side of the acute angle (**Fig. 5(b)**). This geometrical relationship of the streamers can be well understood by considering the formation of dislocation sources through cross-slipping due to the line tension of surface screw dislocations emerging on the side surfaces as a result of movements of the edge components of the multiplied dislocations, which will be discussed in section 4.3.

Close observations on the bright and dark pits in streamers show that they do not lie on the single slip plane, as already shown in **Fig. 4(a)**. This result means that the secondarily formed dislocation sources do not stay on the single slip planes for long time. The number of the plus or minus edge dislocations that form streamers is only approximately 20 in the maximum. In Cu-Al single crystals, on the other hand, Mitchell et al [26, 27] showed that each of the plus and minus edge dislocations which formed streamers appears to lie on the single slip planes as observed by optical microscopy and their number was very large. Their results indicate that in Cu-Al crystals having a lower stacking fault energy than pure Cu, the stability for the dislocation sources to stay on the single slip planes is higher than in pure Cu and also the life time is longer in Cu-Al crystals than in pure Cu.

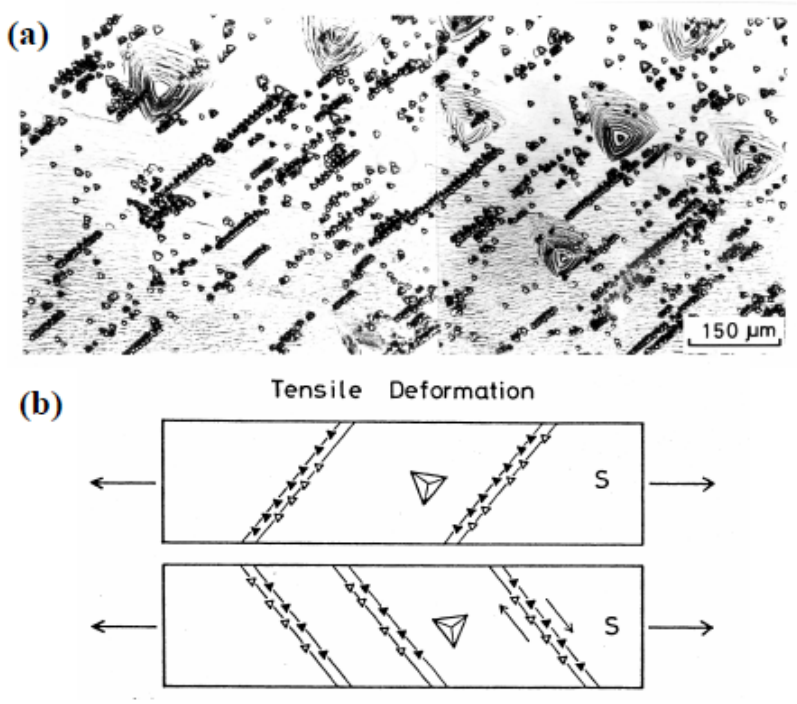

Fig. 5 (a) Streamers, row of edge dislocation dipoles under the stress of 10.6×10^4Pa for 20 seconds at room temperature for specimen U123-6. (b) The location of plus and minus edge dislocation rows forming a streamer produced by tensile loading at room temperature.

4. Discussion

In order to make clear the yielding mechanism of highly perfect copper crystals, we discuss the

character of dislocation sources responsible for the initiation of dislocation multiplication, the controlling mechanism of the multiplication stress, τ_m, equal to the yield stress, and the mechanism of propagation of dislocation multiplication onto the neighboring parallel slip planes.

4.1 The character of trigger dislocation sources

Figure 6 shows a model that may well explain the experimental results obtained so far for the specimens where the grown-in surface edge dislocations are not pinned or weakly pinned by impurities and can move long distances at low stresses below τ_m. The model tells that the dislocation source is formed by the following four successive processes;

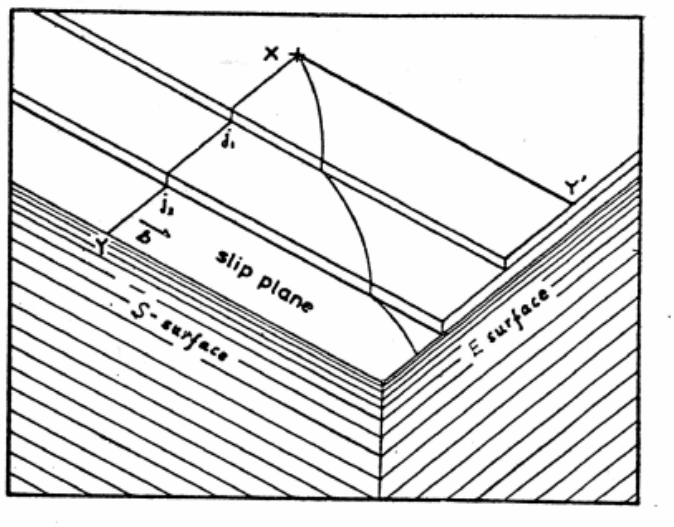

Fig. 6 Transformation of a jogged edge dislocation source Xj_1j_2Y emerging on S-surface into a straight screw dislocation XY' emerging on E-surface. XY' would act as a trigger dislocation for dislocation multiplication.

(1) A primary edge dislocation emerging on the {111} surface (S surface) travels long distance at stresses below τ_m. (2) Giant jogs that exist along the grown-in edge dislocation and are glissile can be swept away out of the side surface (E surface) as a result of long distance motion of the dislocation with the giant jogs. (3) As a result, a pure screw dislocation that terminates at the side surface near the specimen edge and lies on a single slip plane is formed. (4) This secondarily formed pure screw dislocation has a long segment lying on a single slip plane and thus can act as a trigger source under considerably lower stresses than grown-in screw dislocations with giant jogs.

Although the processes (1), (2) and (4) have been experimentally confirmed by the previous [21-23] and present studies, the process (3) has not been confirmed yet. The process (3) suggests that the formation of such a long, pure-screw dislocation is closely related to the readiness of sweep of the giant jogs and hence its preferential formation may occur at places where the giant jogs can be easily swept away out of the specimen. Since the primary slip plane, {111} surfaces and side surfaces are not perpendicular one another, there exist acute and obtuse corners on the slip plane. The giant jogs can be more easily swept away at the acute corner than at the obtuse corner, suggesting a preferential formation of trigger dislocation sources near the acute corner. We have examined the preferential place for the formation of trigger dislocation sources for U123-2 and U123-6.

It has been found that the dislocation sources are formed near not only the acute corner, but also the obtuse corner: For example, the dislocation source for a bright-pit array in **Fig. 4 (a)** is near an obtuse corner. This is very likely because the difference in angle between the obtuse and acute corners with the <123> axis for U123-2 and U123-6 is small, only $\pi/9$ radian. Therefore, specimen U110-2, which has a large difference between the obtuse and acute corners, $\pi/9$ radian, was prepared to examine the formation sites of dislocation sources. In the specimen preparation, special attention was paid to eliminate any irregularity along the four

edges of U110-2 since edge irregularity provides the sites of stress concentration and may work as a preferential site for dislocation multiplication.

Figure 7 shows a dislocation distribution on the $(\bar{1}1\bar{1})$ surface of U110-2 under a stress of $8.1\text{x}10^4$Pa ($\sim\tau_m$) at room temperature for 20 seconds, (a) before and (b) after removing 400μm in depth from the original, as-stressed surface by electro-polishing. The large pits in **Fig. 7(a)** correspond to grown-in dislocations and the small pits in **Fig. 7(a)** and **7(b)** to multiplied dislocations. The small pits were two-fold etched with [A] and then Livingston etchants. It should be noted that the arrays of small etch pits exhibit the outer part of bright contrasts and the inner part of dark contrasts. This contrast of small etch pits means that the multiplied edge dislocation arrays moved from right to left in **Fig. 7** and therefore the dislocation sources for these edge dislocation arrays exist near the right side in the figure. The right side corresponds to an acute corner as seen from the shape of the pits on the $(\bar{1}1\bar{1})$ surface.

From the above discussion, the formation process of dislocation source and the mechanism of the initiation of dislocation multiplication in highly perfect copper crystals can be well explained by the model shown in **Fig. 6**: This is the case for the crystals where the locking stress of grown-in surface dislocations due to impurities such as Cu_2O is low and the grown-in surface edge dislocations can move long distances at stresses below τ_m. In this case a primary surface grown-in edge dislocation travels with giant jogs and sweeps away the giant jogs out of the specimen, transforming to a long, pure screw dislocation lying on a single slip plan. This secondarily formed pure screw dislocation works as a trigger source and causes dislocation multiplication to be initiated.

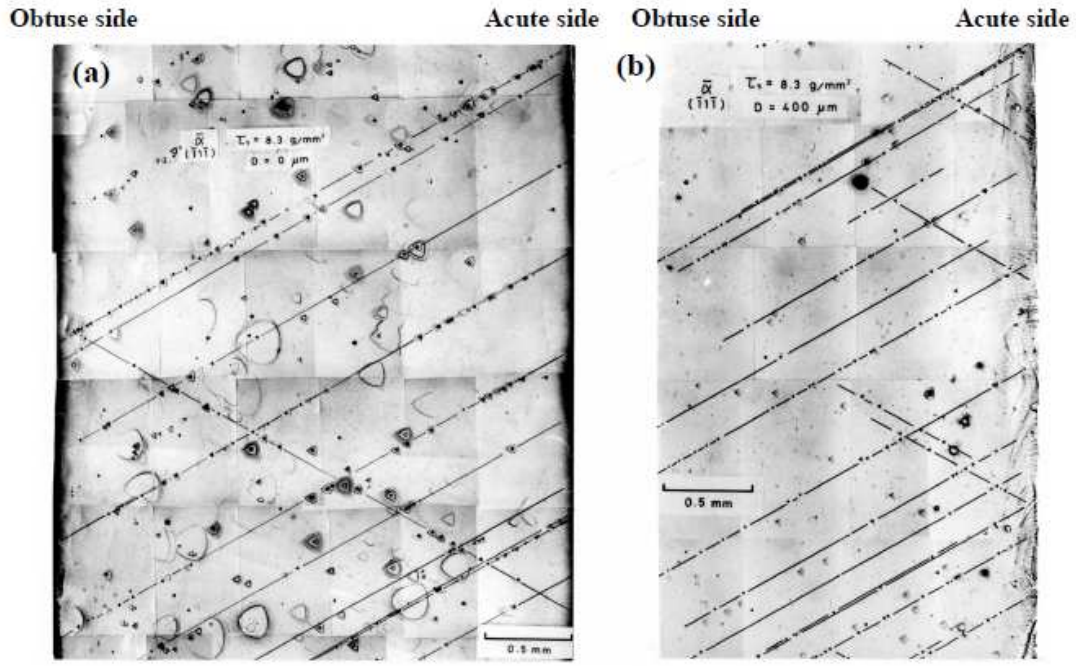

Fig. 7 Arrays of multiplied edge dislocations appearing on the $(\bar{1}1\bar{1})$ surfaces of specimen U110-2 under a stress of $8.1\text{x}10^4$Pa ($\sim\tau_m$), (a) before and (b) after removing 400μm in depth from the original surface by electro-polishing.

On the other hand, in specimen U123-9 of which the impurity locking stress is too high for the grown-in surface edge dislocations to move below τ_m, no long, pure screw dislocations are formed. Since the movement of the grown-in surface 30˚screw dislocations is recognized to occur below τ_m, these screw dislocations may act as a dislocation source and cause dislocation multiplication, yielding highly perfect copper crystals.

4.2 Controlling mechanism of τ_m

It has been found in this study that τ_m is determined by a thermally activated process and is related to the initial dislocation density ρ_0 by eq. (1) in the crystals where the locking stress of grown-in surface edge dislocations is lower than τ_m and their long-distance motion results in the formation of long, pure screw dislocations. In the following, we discuss the elementary process which controls thermally activated process of τ_m.

When the plastic deformation of materials is governed by a thermally activated process of dislocation motion, the plastic shear strain rate $\dot{\gamma}$ is expressed by

$$\dot{\gamma} = \dot{\gamma}_0 exp\{-(U_0 - V\tau_e)/kT\}, \tag{2}$$

where $\dot{\gamma}_0$ is the frequency factor proportional to the thermal vibration, number density of activation sites and area per one activation process swept by dislocation motion, U_0 the activation energy for the dislocation to overcome obstacles, V the activation volume, τ_e the stress acting effectively for thermally activated glide motion of dislocations and $\tau_e = \tau_a - \tau_i$ (τ_a is the applied shear stress, τ_i is the internal stress), k the Boltzmann constant and T the absolute temperature.

In the highly perfect copper crystals, the density of other dislocations that are responsible for τ_i is very low and thus $\tau_e =\sim \tau_a$. In addition, the plastic shear strain rate at τ_m is assumed to be almost identical to ones for all the specimens used, because τ_m was determined as the applied shear stress under which an array of a few arrays of multiplied dislocations composed of about 10 dislocations was at first observed as those of etch pits on a {111} surface. Furthermore, the values of τ_m at room temperature (293K) and 77K were measured for the same specimen of U123-2 in which the microstructure at both temperatures such as the distribution of impurity and the configuration of grown-in dislocation is the identical. Therefore, each of $\dot{\gamma}_0$, V and $\dot{\gamma}$ at 77K is almost equal to that at 293K in eq. (2), and $U_0 = 18.3\text{x}10^4 V$ is obtained. By putting the values of U_0 and τ_m (= τ_e) at 77K and 293K into eq. (2), the activation energy for the specimen with τ_m=9.0x10^{4}Pa measured at 293K follows eq.(3), or

$$U_0 - 9.0x10^4 V = 0.51U_0. \tag{3}$$

When thermal activation occurs at our observable rates at room temperature, the activation energy of 7x10^{-20}J[22] was obtained. Assuming that $0.51U_0$ = 7x10^{-20}J, it follows that $U_0 \approx$1.5x10^{-19}J is the energy required for dislocation multiplication to initiate.

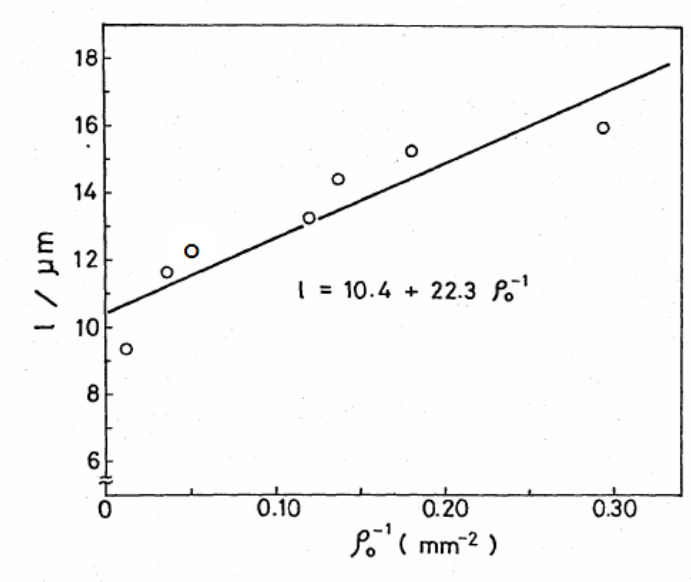

Fig. 8 Relationship between ℓ, obstacle spacing at the multiplication stress, τ_m, and ρ_0^{-1} for ρ_0 = 3.4x10^2～8.3x10^3 cm^{-2}.

Since in eq.(2) $\dot{\gamma}$ at τ_m is constant, $U_0 - \tau_m V = 0.51U_0$ and $V = \ell b^2$ (ℓ is the obstacle spacing at the initiation of dislocation multiplication), the following relation is obtained between ℓ and τ_m.

$$\ell = 0.51U_0/\tau_m b^2 = 130/\tau_m \quad (\mu m). \tag{4}$$

A plot of ℓ estimated from eq.(4) against ρ_0^{-1} leads to the following linear relationship between ℓ and ρ_0^{-1} when $\rho_0 = 3.4\text{x}10^2 \sim 8.3\text{x}10^3 \text{cm}^{-2}$ (**Fig. 8**),

$$\ell = 10.4 + 22.3\rho_0^{-1} \quad (\mu m) \tag{5}$$

The values of ℓ obtained from eq. (5) are one or two orders smaller than the spacing between the forest dislocations obtained by $\rho_0^{-1/2}$, suggesting the obstacles that give such small values of ℓ.

Now, we estimate the distance between jogs, ℓ_{DJ}, on a leading screw dislocation formed by cutting grown-in forest dislocations intersecting with the active primary slip plane in U123-2 ($\rho_0 = 1\text{x}10^3\text{cm}^{-2}$, the primary slip plane: 4.6mm x 4.5mm), while a secondarily formed screw dislocation acts as a trigger source and traverse the primary slip plane. When the grown-in dislocations distribute homogeneously on each slip system, the probability that a jog is formed on the leading screw dislocation by cutting forest dislocations intersecting with the active primary slip plane is 2/3. In addition, when the increase in the forest dislocations density due to their bowing out at the stress of τ_m is assumed to be $\sim 2\rho_0$, the value of ℓ_{DJ} becomes $\ell_{DJ} = 4.5\text{x}10^3/\{(2\text{x}10^3\text{x}0.46\text{x}0.45\text{x}(2/3)) = 16\mu m$, which is close to $\ell = 13\mu m$ obtained from eq.(5) with $\rho_0 = 1\text{x}10^3\text{cm}^{-2}$.

On the other hand, for the specimens having ρ_0 lower than $1\text{x}10^3\text{cm}^{-2}$, e.g., U110-2 ($\rho_0 = 3.4\text{x}10^2\text{cm}^{-2}$) ℓ_{DJ} is estimated to be 120μm, which is much larger than $\ell = 8.4\mu m$ obtained for U110-2 (**Fig. 8**). According to Young et al [28], in crystals with a very low initial dislocation density, such as $\rho_0 < 10^3\text{cm}^{-2}$, furnace cooling after annealing resulted in formation of dislocation loops by the condensation of excess vacancies. Assuming that the number density of dislocation loops is approximately $4\text{x}10^5\text{cm}^{-3}$ for $\rho_0 = 1\text{x}10^2\text{cm}^{-2}$ [28], use of this loop density and the dimensions of the primary slip plane in U110-2 (3.2mmx3.6mm) leads to $\ell_{LJ} = 3.2\text{x}10^3/\{(4\text{x}10^5)^{2/3}\text{x}(1/2)\text{x}2\text{x}0.32\text{x}0.36\} = 5.5\mu m$. This value is close to the above mentioned one (8.4μm).

It has been widely accepted that the formation energy of a vacancy is $1.6\text{x}10^{-19}$J and the activation energy for self-diffusion is $3.4\text{x}10^{-19}$J [29] for copper crystals. Therefore, the above-estimated activation energy for deformation, U_0, is close to the vacancy formation energy. Seeger [30] has proposed that since jogs on a screw dislocation move conservatively along the screw dislocation line and move away from the created vacancy, the binding force between jogs and the vacancy is negligibly small and thus the activation energy for movement of jogs on a screw dislocation should be equal to the formation energy of a vacancy. Therefore, U_0 is very likely corresponding to be the activation energy for non-conservative motion of jogs on the screw dislocation in the sense of the above model by Seeger. In addition, this model may well explain the other experimental results, such as the slower movement of screw dislocations than that of edge ones.

In conclusion, in the specimen of the highly perfect copper crystals where the grown-in edge dislocations are not pinned or weakly pinned and do pre-yield long distance motion at stresses below τ_m, the value of τ_m is determined by non-conservative motion of jogs on the leading multiplied screw dislocation formed by cutting forest dislocations and/or vacancy loops intersecting with the active primary slip plane; the non-conservative motion of jogs on the screw dislocation is described here as Seeger's model.

On the other hand, in specimen U123-9 where the grown-in edge dislocations are strongly pinned and cannot do pre-yield long distance motion below τ_m, the value of τ_m was 1.8 times as high as the stress expected from eq (1) and the grown-in screw dislocation with less pinning most likely acted as the trigger dislocation source. The grown-in dislocations were reported to have large super-jogs of 10μm in height [19]. However, it is very unlikely that a thermally activated process forms the amount of vacancies equivalent to the height of the large super-jogs, and the non-conservative motion of such large super jogs cannot be expected to occur near room temperature. Therefore, it is reasonable to state that in U123-9 the value of τ_m is determined by the stress required for free segments between super-jogs of grown-in screw dislocations to operate as a trigger dislocation source.

4.3 Mechanism of propagation of dislocation multiplication

It has been revealed in the present study that the side {145} surfaces for 123-Specimen, where the primary screw dislocations emerge, play a vital role on the formation of dislocation sources responsible for the propagation of dislocation multiplication onto the neighboring parallel slip planes. It has been also found that there is a certain geometrical relation between the primary slip plane activated for the initiation of dislocation multiplication and that followed by the propagation of dislocation multiplication. These results indicate that the propagation of dislocation multiplication onto the neighboring parallel slip planes occurs through the double cross slip of multiplied screw dislocations at the side {145} surfaces.

The edge components of the primary multiplied dislocations emitted from the trigger dislocation source move and reach the {145} surface from $(1\bar{1}1)$ surfaces, emerging on the {145} surface as pure screw dislocations. For the pure screw dislocations, the primary slip plane deviates by $\pi/18$ radian from the direction perpendicular to the {145} surface and the cross-slip plane is parallel to the $(1\bar{1}1)$ surface. Since extended dislocations shrink near surfaces[31], the multiplied screw dislocations that emerge on the {145} surface are very likely to cross-slip so as to lie perpendicularly to the {145} surface by the aids of the line tension and stress concentration from the following dislocations. When the cross-slipped screw dislocations do double cross slip onto the slip planes parallel to the original one, the double cross-slipped screw dislocations can work as new dislocation sources near the {145} surface. As a result, dislocation multiplication occurs on the. The multiplied dislocations emitted from the new dislocation sources move on the slip planes parallel and close to the original slip plane and reach the $(1\bar{1}1)$ surface from the {145} surface and can be observed as edge dislocations moving in the direction opposite to that during the initiation of dislocation multiplication.

Moving dislocations multiplied from the trigger source and those from the source formed by double-cross slip pass away each other on the individual parallel slip planes distant by h. When h is less than the following critical distance, h_C,

$$h_C = \mu b/8\pi\nu\tau_m \quad \text{(edge dislocations) and}$$
$$h_C = \mu b/4\pi\tau_m \quad \text{(screw dislocations),}$$

streamers are formed. Here, μ is the shear modulus and ν the Poisson ratio. In this case streamers should be most frequently formed near the {145} surface where new dislocation sources are formed by double cross slip of surface screw dislocations or near the specimen edge intersecting with the {145} and $(1\bar{1}1)$ surfaces.

When cross slip occurs due to the line tension, it is possible to predict the direction of cross slip and the geometrical relationship between the primary slip planes originally activated and subsequently activated after double cross slip. As shown in section 3.2, the predicted relationship has been confirmed to agree well with that between the bright and dark pits composed of the streamers in **Fig. 5**.

In conclusion, the process of propagation of dislocation multiplication onto the parallel slip planes is described as follows: The edge components of the primary multiplied dislocations that are emitted from the trigger source move and reach the {145} surface from the $(1\bar{1}1)$ surface, emerging on the side {145} surface as screw dislocations. The screw dislocations do double cross slip onto the slip planes parallel to the original one at the {145} surface by the aids of line tension and stress concentration from the following dislocations. As a result, the multiplied screw dislocations can work as new dislocation sources and chain-reaction-like production of such dislocation sources causes the propagation of dislocation multiplication onto the neighboring parallel slip planes.

5. Conclusions

In order to make clear the yielding mechanism of highly perfect copper crystals, the behavior of dislocation multiplication has been investigated by using etch pit techniques for crystals with no or few sub-grain boundaries and very low initial dislocation densities from $3.4\text{x}10^2$ to $8.3\text{x}10^3\text{cm}^{-2}$. The following conclusions have been obtained.

1. In crystals where grown-in surface dislocations are weakly pinned by impurities such as Cu_2O, the surface edge dislocations move long distances below the multiplication stress, τ_m, and sweep away their large super-jogs from the crystals, transform into elongated, fresh screw dislocations terminating at the free side

surface near the specimen edge and containing no super-jogs. Such a screw dislocation acts as a trigger source responsible for the yielding.

2. In the weakly pinned crystals, τ_m depends strongly on temperature and loading time showing a thermally activated process. Thus, τ_m at room temperature is expressed by the following relationship with the initial dislocation density, ρ_0,

$$\tau_m = 8.6 \times 10^4 + 6.7\rho_0 \quad \text{(Pa)}.$$

3. τ_m is determined by the non-conservative motion of jogs of a leading screw dislocation multiplied from the trigger source. The jogs are formed by cutting reaction of the screw dislocations with forest dislocations and/or vacancy loops intersecting with the active primary slip plane.

4. In crystals where grown-in edge dislocations are strongly pinned, yielding begins after unpinning of grown-in surface 30°screw dislocations that are less pinned than the grown-in edge dislocations.

5. The value of τ_m for the pinned crystals is 1.8 times as high as that expected form the equation between τ_m and ρ_0 for the unpinned crystals, which is derived based on the stress required for free segments between super-jogs of grown-in screw dislocations to operate as a trigger dislocation source.

6. The propagation of dislocation multiplication onto the neighboring parallel slip planes is triggered by dislocation sources which are produced through the double cross-slip of screw dislocations at the free surfaces.

Acknowledgments

The authors would like to express their sincere gratitude to Prof. C. Kinoshita, Kyushu University for his review of the paper.

References

1) F. W. Jr Young; On the Yield Stress of Cu, J. Appl. Phys., 33, 963-969 (1962).
2) P. Petroff, J. Washburn; Influence of Jog Concentration on the Conservative Motion of Dislocations in Cu, J. Appl. Phys., 37, 4987-4990 (1966).
3) K. Marukawa, Dislocation Motion in Copper Single Crystals, J. Phys. Soc. Japan, 22, 499-510 (1967).
4) T. Suzuki, Lattice Defects and Mechanical Properties in Metals, edited by Japan Inst. Metals, Maruzen, p. 222 (1967).
5) S. Kitajima; Bull. Japan Inst. Metals, 6, 691 (1967).
6) F. W. Jr. Young, F. A. Sherrill; Studies of Dislocations in Lightly Deformed Single Crystals by Ballmann X-Ray Topography, Canad. J. Phys., 45, 757-763 (1967).
7) B. W. T. Rydges; Phil. Mag., 17, 1079 (1968).
8) L. Johnson, M. F. Ashby; Acta Met., 16, 219 (1968).
9) F. W. Jr.Young; Dislocation Dynamics, MaGraw-Hill, New York, p. 313 (1968).
10) S. Kitajima, H. Tonda, H. Kaieda; Dislocation Motion and Multiplication in Copper Crystals, Proc. Int. Conf. on Strength of Metals and Alloys, Supplement to Trans. Japan Inst. Metals, 9, 740-746 (1968).
11) K. Marukawa; Yield Strength and Dislocation Motion in Pure Copper Single Crystals, Bull. Japan Inst. Metals, 8, 569-575 (1969).
12) F. W. Jr Young, F. A. Sherrill; J. Appl. Phys., 42, 230 (1971).
13) M. Ohta, S. Kitajima, K. Aoyanagi, H. Kaieda; Dislocation Motion and Distribution Before and Just After Yielding in a Copper Single Crystal, J. Japan Inst. Metals, 35, 929-936 (1971).
14) M. Ohta, S. Kitajima, H. Kaieda; Dislocation Density and Crystal Size Effects on the Yielding Behavior of Copper Crystals, J. Japan Inst. Metals, 36, 617-622 (1972).
15) F. W. Jr.Young, F. A.Sherrill; J. Appl. Phys., 43, 2949 (1972).
16) H. Tonda, S. Kitajima, H. Kaieda; Yielding of Highly Perfect Copper Crystals, J. Japan Inst. Metals, 37, 164-172 (1973).
17) S. Kitajima; Bull. Japan Inst. Metals, 13, 105 (1974).
18) S. Kitajima; Role of Free Surface on Yielding and Easy Glide Deformation in Highly Perfect Copper Crystals, Surface Effects in Crystal Plasticity, Noordhoff-Leyden, p.495 (1977).
19) H. Kurishita, S. Kitajima; Refinement of an Etch Pit Technique and a Study of Dislocation Configuration

near Surface in Well-Annealed Copper Crystals, J. Japan Inst. Metals, 42, 973-980 (1978).
20) S. Kitajima, M. Ohta, H. Tonda; Production of Highly Perfect Copper Crystals by Thermal Cyclic Annealing, J. Crystal Growth, 24/25, 521-526 (1974).
21) H. Kurishita, S. Kitajima; The Beginning of Motion of Dislocations in Highly Perfect Copper Crystals, Japan Inst. Metals, 43, 364-371 (1979).
22) H. Kurishita, S. Kitajima; Motion of Dislocations in Highly Perfect Copper Crystals, J. Japan Inst. Metals, 43, 372-380 (1979).
23) H. Kurishita, S. Kitajima; Yielding of Highly Perfect Copper Crystals, Strength of Metals and Alloys, Vol.1, p.101-106 (1979).
24) Y. Miura, F. Higuchi; Dislocation Multiplication Sources in Copper Revealed by X-ray Topography, Phil. Mag., 71, 1363-1373 (1995).
25) J. D. Livingston; Direct Observations of Imperfections in Crystals, Interscience Publishers, New York, p.115 (1962).
26) J. W. Mitchell, J. C. Chevrier, B. J. Hockey, J. P. Jr. Monghan; Can. J. Phys., 45, 453 (1967).
27) B. J. Hockey, J. W. Mitchell, Phil. Mag., 26, 409 (1972).
28) F. W. Jr. Young, T. O. Baldwin, F. A. Sherrill; Lattice Defects and Their Interaction, Ed. by R. R. Hashiguchi, Gordon and Breach, New York, p.543 (1967).
29) M. Mehrer, A. Seeger; Phys. Status Solidi, 35, 313 (1969).
30) A. Seeger; Phil. Mag., 46, 1194(1955).
31) E. Winter, H. P. Karnthaler, P. M. Hazzledine; Surface Effects in Crystal Plasticity, Noordhoff-Leyden, p.927 (1977).